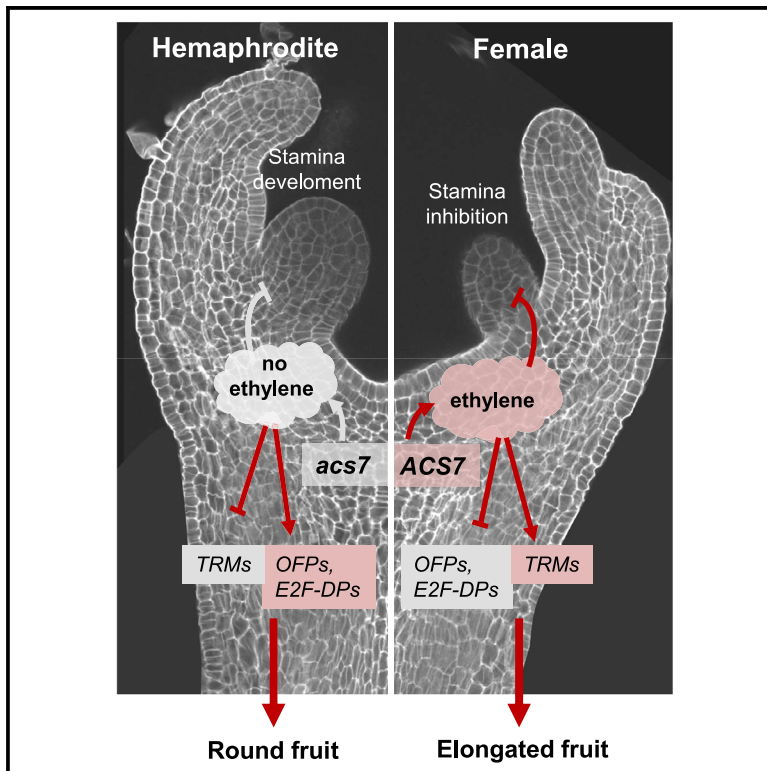


# Current Biology

## Ethylene plays a dual role in sex determination and fruit shape in cucurbits

### Graphical abstract



### Authors

Adnane Boualem, Serge Berthet, Ravi Sureshbhai Devani, ..., Nebahat Sari, Catherine Dogimont, Abdelhafid Bendahmane

### Correspondence

abdelhafid.bendahmane@inrae.fr

### In brief

Flowers and fruits are essential for angiosperm seed production and dispersal. By investigating the mechanisms controlling unisexual flower development and fruit shape, Boualem et al. reveal a dual role of ethylene in female flower development and fruit elongation. These processes implicate the control of cell elongation and cell division.

### Highlights

- *Cucumis melo round fruit 1* encodes a null allele of *CmACS7*
- Fruit shape is determined after sex determination and before flower stage 8
- Melon germplasms show strong association between fruit shape and sexual types
- Ethylene regulates *E2F-DP*, *OVATE*, and *TRM5* modules to control fruit shape

Article

# Ethylene plays a dual role in sex determination and fruit shape in cucurbits

Adnane Boualem,<sup>1,3</sup> Serge Berthet,<sup>1</sup> Ravi Sureshbhai Devani,<sup>1</sup> Celine Camps,<sup>1</sup> Sebastien Fleurier,<sup>1</sup> Halima Morin,<sup>1</sup> Christelle Troadec,<sup>1</sup> Nathalie Giovinozzo,<sup>2</sup> Nebahat Sari,<sup>2</sup> Catherine Dogimont,<sup>2</sup> and Abdelhafid Bendahmane<sup>1,4,\*</sup>

<sup>1</sup>Université Paris-Saclay, CNRS, INRAE, Université Evry, Institute of Plant Sciences Paris-Saclay (IPS2), 91190 Gif sur Yvette, France

<sup>2</sup>INRAE GAFL, Génétique et Amélioration des Fruits et Légumes, 84143 Montfavet, France

<sup>3</sup>Twitter: @AdnaneBoualem

<sup>4</sup>Lead contact

\*Correspondence: [abdelhafid.bendahmane@inrae.fr](mailto:abdelhafid.bendahmane@inrae.fr)

<https://doi.org/10.1016/j.cub.2022.04.031>

## SUMMARY

Shapes of vegetables and fruits are the result of adaptive evolution and human selection. Modules controlling organ shape have been identified. However, little is known about signals coordinating organ development and shape. Here, we describe the characterization of a melon mutation *rf1*, leading to round fruit. Histological analysis of *rf1* flower and fruits revealed fruit shape is determined at flower stage 8, after sex determination and before flower fertilization. Using positional cloning, we identified the causal gene as the monoecy sex determination gene *CmACS7*, and survey of melon germplasms showed strong association between fruit shape and sexual types. We show that *CmACS7*-mediated ethylene production in carpel primordia enhances cell expansion and represses cell division, leading to elongated fruit. Cell size is known to rise as a result of endoreduplication. At stage 8 and anthesis, we found no variation in ploidy levels between female and hermaphrodite flowers, ruling out endoreduplication as a factor in fruit shape determination. To pinpoint the gene networks controlling elongated versus round fruit phenotype, we analyzed the transcriptomes of laser capture microdissected carpels of wild-type and *rf1* mutant. These high-resolution spatiotemporal gene expression dynamics revealed the implication of two regulatory modules. The first module implicates *E2F-DP* transcription factors, controlling cell elongation versus cell division. The second module implicates *OVATE*- and *TRM5*-related proteins, controlling cell division patterns. Our finding highlights the dual role of ethylene in the inhibition of the stamina development and the elongation of ovary and fruit in cucurbits.

## INTRODUCTION

Fruit, the mature ovary of a flower, is a vital structure in the sexual life cycle of angiosperms. Fruit development is initiated by ovule fertilization, which promotes the ovary wall to undergo development and differentiation into fleshy or dry fruits. At maturity, fruits enclose and protect seeds and aid in their dispersal. In angiosperms, fruit initiation and development share evolutionarily conserved biological processes but at maturity exhibit an extraordinary diversity in terms of color, size, and shape. This diversity is driven by Darwinian natural selection and thousands of years of artificial selection of fruit traits relevant to fruit production and marketing. For instance, fruit attributes such as size and shape are important in fruit harvesting and packaging, with consequences on transportation. Fruit appearance also has a major influence on consumers, who prefer fruits of equal weight and uniform shape.<sup>1</sup>

Fruit shape is the result of coordinated spatiotemporal regulation of cell division and expansion. The genetic basis of fruit shape has been assigned to a limited number of genes in several crops.<sup>2–8</sup> In tomato, a model species of fruit shape, five genes have been shown to control fruit shape and development: *FASCIATED* (*FAS*); *LOCULE NUMBER* (*LC*); *SUN*; *OVATE*,

*ovate-family protein* (*SIOFP20*), and *TONNEAU1-RECRUITING MOTIF 5* (*SITRM5*).<sup>9–14</sup> *LC* and *FAS*, orthologs of *WUSCHEL* and *CLAVATA3* transcription factor (TF), respectively, influence the tomato fruit shape through the regulation of the number of fruit locules.<sup>9,11,15</sup> *SUN*, a member of the IQ67 domain (IQD) protein family, positively regulates fruit elongation.<sup>12,16,17</sup> *OVATE*, the founding member of the *OVATE*-family proteins (OFPs), encodes a protein with a conserved ~70 amino acid C-terminal domain, the *OVATE/DUF623* domain.<sup>18</sup> Wild-type (WT) *OVATE* and *SIOFP20* regulate fruit shape through repression of cell division in the longitudinal axis and enhance cell division along the transversal axis.<sup>10,14,19</sup> *SITRM5*, a member of the Arabidopsis *TRM1-5* clade, interacts with *OVATE* to regulate cell division in developing ovaries.<sup>14</sup>

The *Cucurbitaceae* is one of the angiosperm families with the most diverse fruits. For instance, fruit size of wild melon (*Cucumis melo* var. *agrestis*) and cucumber (*Cucumis sativus* var. *hardwickii*) is quite small, weighing less than 50 g.<sup>20</sup> By contrast, the *Atlantic Giant* variety of pumpkin (*Cucurbita maxima*) holds the world record for fruit weight, reaching 1,056 kg.<sup>21</sup> Fruit shape is also very diverse. Fruits of the *flexuosus* melon varieties can reach more than 2 m length with a fruit growth rate of 9 cm per day.<sup>22</sup> Fruit shape is also very diverse in bottle gourd and squash

(*Cucurbit pepo*) with spherical, cylindrical, elongated, curved, oblate, obovoid, drum-shaped, pear-shaped, spindle-shaped, or crooked neck forms.<sup>23,24</sup> Owing to this extraordinary diversity of fruit shapes and sizes, *Cucurbitaceae* are excellent model systems to understand the molecular mechanisms governing fruit development.

Several studies have reported major quantitative trait loci (QTLs) controlling cucurbit fruit shapes.<sup>1,2,25–27</sup> In cucumber, *CsFUL1*, *short fruit 1* (SF1), and *SF2* encode a FRUITFULL-like MADS-box TF, a cucurbit-specific RING-type E3 ligase, and a histone deacetylase complex 1 homolog, respectively.<sup>28–30</sup> *CsFUL1* represses the expression of *CsSUPERMAN* and inhibits auxin transport and thereby regulates cell division and expansion.<sup>30</sup> In melon, the fruit shape QTL *fsqs8.1/CmFSI8* encodes an OFP, CmOFP13, orthologous to SIOFP20.<sup>31,32</sup>

Interestingly, some of the cucurbit fruit shape QTLs were shown to be associated with sex determination genes.<sup>2,3,33</sup> In melon, the fruit shape QTL *fs2.2* co-segregates with the *Monoecy* (separate male and female flowers on the same plant) gene, *CmACS7*, encoding for 1-aminocyclopropane-1-carboxylic acid synthase, the rate-limiting enzyme in ethylene biosynthesis.<sup>1,2,34</sup> Similarly, in cucumber, the QTL controlling the transition between elongated and round fruit co-segregates with *CmACS7* orthologous gene, *CsACS2*.<sup>3,33,35</sup> Ethylene is also a key hormone in higher plants commonly associated with fruit ripening.<sup>36,37</sup> Although genetic associations between *Cucurbitaceae* sex determination genes and fruit development have been proposed, little is known about the link between sex determination, ethylene production, and cellular and molecular mechanisms involved in *Cucurbitaceae* fruit shape determination.

Here, we report the cloning and characterization of a new melon mutant, *round fruit 1* (*rf1*), which encodes a null allele of *CmACS7*. We reveal how ethylene produced by *CmACS7* controls cell division and elongation, providing mechanistic insights into fruit shape regulation in plants.

## RESULTS

### Elongated versus round fruit shapes are determined before flower anthesis

The melon inbred line Charentais Mono is a monoecious breeding line producing elongated fruit. To identify genes controlling fruit shape, we produced an ethyl methanesulfonate (EMS) mutagenized collection from the Charentais Mono line. Phenotyping of 10,000 M2 plants corresponding to 1,000 M2 families led to the identification of one mutant with rounded fruits (*rf1*; Figures 1A and 1B). To measure the roundness of *rf1* fruits, we calculated the fruit shape index (FSi) as the ratio of the fruit length by the fruit diameter at mature stage. We found fruit length significantly longer in the Charentais Mono line (WT) compared with *rf1* mutant. In contrast, fruit diameter did not significantly differ (Figures 1C and 1D), leading to FSi of 1.59 for the WT and 1.34 for the *rf1* mutant (Figure 1E). To pinpoint when melon fruit shape is determined, we measured FSi of the developing fruits of WT and *rf1* plants, starting from fertilized flower at anthesis stage to mature fruit (Figure S1). We found significant differences of FSi between WT and *rf1* plants at all investigated fruit developmental stages, suggesting that melon fruit shape

is determined before flower fertilization (Figures S1A–S1C). To validate this, we measured the ovary shape index (OSi) as the ratio of the ovary length by the ovary width at anthesis stage and before flower fertilization. As for the fruits, we found ovary length significantly longer in WT compared with *rf1* mutant and no significant difference in the width of the ovaries (Figures 1F–1J), leading to OSi of 2.58 for the WT and 1.95 for the *rf1* mutant (Figure 1J). Based on this, we concluded that elongated versus round fruit shape is determined during ovary development and before flower fertilization.

To investigate the inheritance of the round fruit phenotype, *rf1* plants were back crossed to WT. Consistent with *rf1* being a recessive mutation, F1 hybrid plants developed elongated fruits with FSi similar to WT plants (Figures 1C–1E). Analysis of the F2 population showed 3:1 segregation of elongated versus round fruit phenotypes, consistent with the hypothesis that *rf1* is a single-locus recessive mutation leading to round fruit (Table S1).

### *rf1* locus encodes 1-aminocyclopropane-1-carboxylic acid synthase

To identify *rf1* causal mutation, we sequenced bulked-genomic DNA from M2 plants producing elongated fruits versus round fruits and determined the delta-SNP index. Four SNPs with  $\Delta$ (SNP index) superior to 0.5 and mapping to chromosome 2 telomeric region were found linked to *rf1* (Figure 1K). Fine mapping further delimited *rf1* to G1504A transition leading to D279N missense mutation in the sex determination gene *CmACS7* (Figures 1L and 1M). Primary and tertiary protein structure analysis revealed D279N amino acid modification altering a highly conserved protein domain, implicated in the binding of the enzyme cofactor, the pyridoxal 5'-phosphate (PLP)<sup>38,39</sup> (Figures 1N, S2A, and S2B). To investigate whether D279N mutation affects *CmACS7* enzymatic activity, we expressed His-tagged recombinant *CmACS7* and *CmACS7*<sup>D279N</sup> proteins and assayed their activity *in vitro* by monitoring 5'-methylthioadenosine (MTA) formation at different PLP concentrations. The enzymatic assays showed that *CmACS7*<sup>D279N</sup> displays very low ACS activity at all PLP concentrations (Figure 1O). These results indicate that *CmACS7*-mediated ethylene production likely leads to the development of elongated fruits, whereas loss of enzymatic activity leads to round fruits.

Previously, we showed that *CmACS7* plays a major role in sex determination and that loss of *CmACS7* enzymatic activity leads to the female to hermaphrodite sexual transition.<sup>40</sup> Consistent with this, we found *rf1* plants andromonoecious, developing male and hermaphrodite flowers (Figure S1). To further test the correlation between the development of female flowers and elongated fruit, we phenotyped our previously reported *CmACS7* mutants, *CmACS7*<sup>G19E</sup>, *CmACS7*<sup>A57V</sup>, and *CmACS7*<sup>D376N</sup>, for fruit shape. *CmACS7*<sup>G19E</sup> and *CmACS7*<sup>A57V</sup> isoforms showed reduced ACS enzymatic activity, whereas the *CmACS7*<sup>D376N</sup> isoform is mutated in a nonconserved amino acid position predicted to not impair the protein function<sup>40</sup> (Figure S2C). We found that all the mutations leading to female to hermaphrodite flower sexual transition also lead to round fruit development (Figures S1D–S1S). Conversely, the mutation *CmACS7*<sup>D376N</sup>, not altering sex of the flower, does not alter fruit shape.

To test whether this correlation occurs also in cucumber, we phenotyped five *CsACS2* mutants for fruit development.<sup>41</sup>

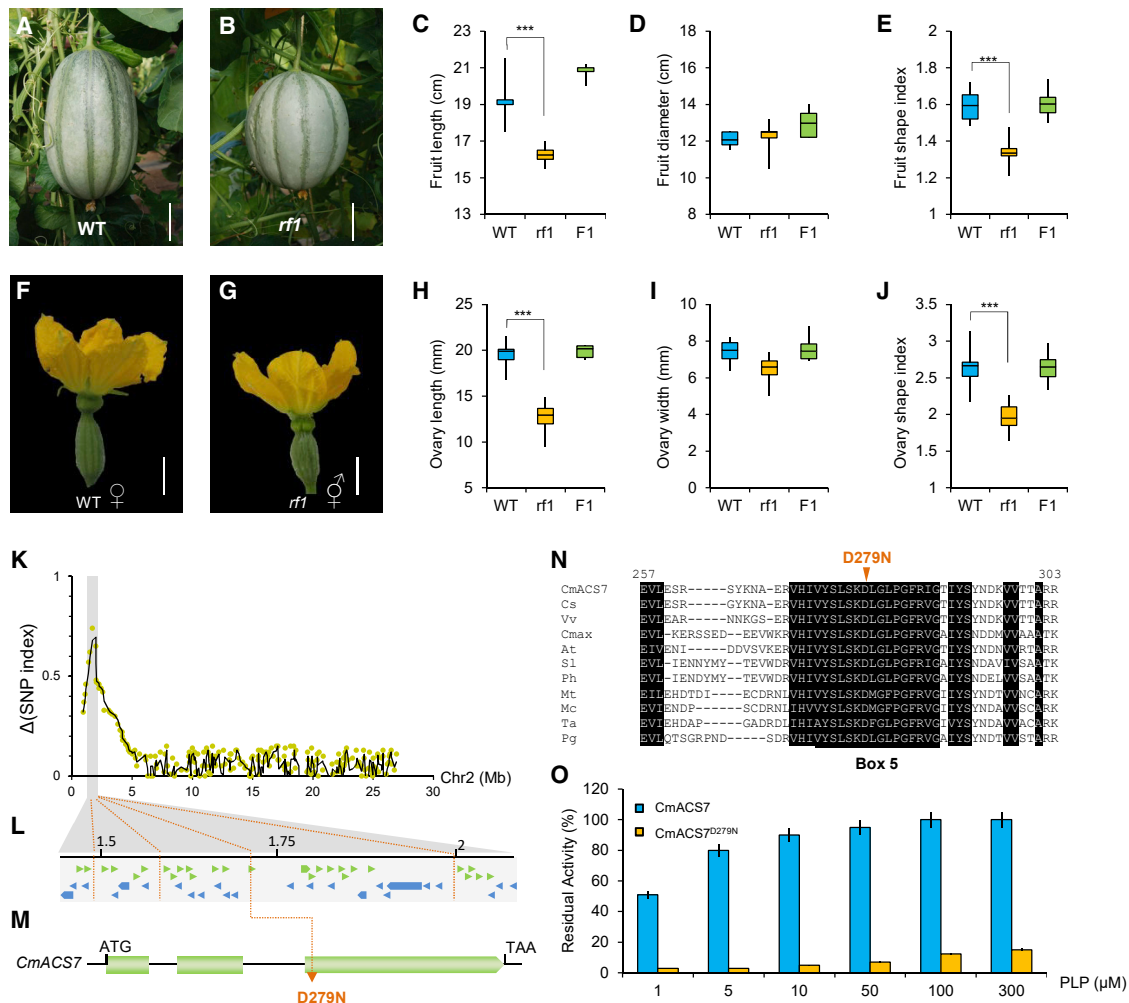


**Figure 1. *rfl* develops round fruit and encodes *CmACS7***

(A and B) Elongated (A) and round (B) fruit developed on WT and *rfl* mutant plant, respectively. Scale bars, 5 cm.

(C–E) Boxplots of fruit length (C), fruit diameter (D), and fruit shape index (E) in the WT, *rfl*, and F1 plants (n = 10).

(F and G) Flowers of WT (F) and *rfl* (G) plants at anthesis. Scale bars, 1 cm.

(H–J) Boxplots of ovary length (H), ovary width (I), and ovary shape index (J) in the WT, *rfl*, and F1 plants (n = 20).

Data in (C)–(E) and (H)–(J) are displayed as boxplot whiskers representing  $\pm 1.5\times$  the interquartile range; horizontal lines, medians. \*\*\*p < 0.001 (two-tailed Student's t test).

(K–M) Cloning of the *rfl* locus.

(K) The delta-SNP index ( $\Delta$ SNP index) between elongated and round bulks.

(L) Schematic of the mapping region of the *rfl* locus. The green and blue arrows represent annotated genes. Orange dashed lines indicate the physical position of the induced EMS mutations.

(M) Structure of the *CmACS7* gene and position of the missense induced mutation D279N. Green boxes and black lines represent exons and introns, respectively.

(N) Amino acid alignments of *CmACS7* with homologous proteins from *Cucumis sativus* (Cs), *Vitis vinifera* (Vv), *Cucurbita maxima* (Cmax), *Arabidopsis thaliana* (At), *Solanum lycopersicum* (Sl), *Petunia hybrida* (Ph), *Medicago truncatula* (Mt), *Momordica charantia* (Mc), *Triticum aestivum* (Ta), and *Picea glauca* (Pg). Numbers above the alignment indicate the amino acid positions along the *CmACS7* protein. Box 5 indicates a conserved domain in ACS proteins.

(O) Effect of PLP concentration on the ACS enzymatic activity of *CmACS7* (blue bars) and D279N (orange bars) protein forms.

See also [Figures S1–S3](#) and [Table S1](#).

CsACS2<sup>G33C</sup>, CsACS2<sup>P209S</sup>, and CsACS2<sup>S399L</sup> isoforms showed reduced to no ACS enzymatic activity whereas CsACS2<sup>S238F</sup> and CsACS2<sup>S249F</sup> isoforms are impaired in nonconserved amino acid positions predicted to not impact the protein function.<sup>41</sup> As in melon, CsACS2 loss-of-function mutants, CsACS2<sup>G33C</sup>, CsACS2<sup>P209S</sup>, and CsACS2<sup>S399L</sup>, developed hermaphrodite flowers and round fruits, whereas mutants not impaired in ACS

activity, CsACS2<sup>S238F</sup> and CsACS2<sup>S249F</sup>, developed female flowers and elongated fruits ([Figure S3](#)). As the loss of the enzymatic activity of *CmACS7*/*CsACS2* is associated with round fruit development, ethylene is likely a positive activator of elongated fruit growth. To test this hypothesis, we treated monoecious melon plants with 400 ppm of the ethylene perception inhibitor, silver nitrate, and phenotyped the developed fruits for fruit

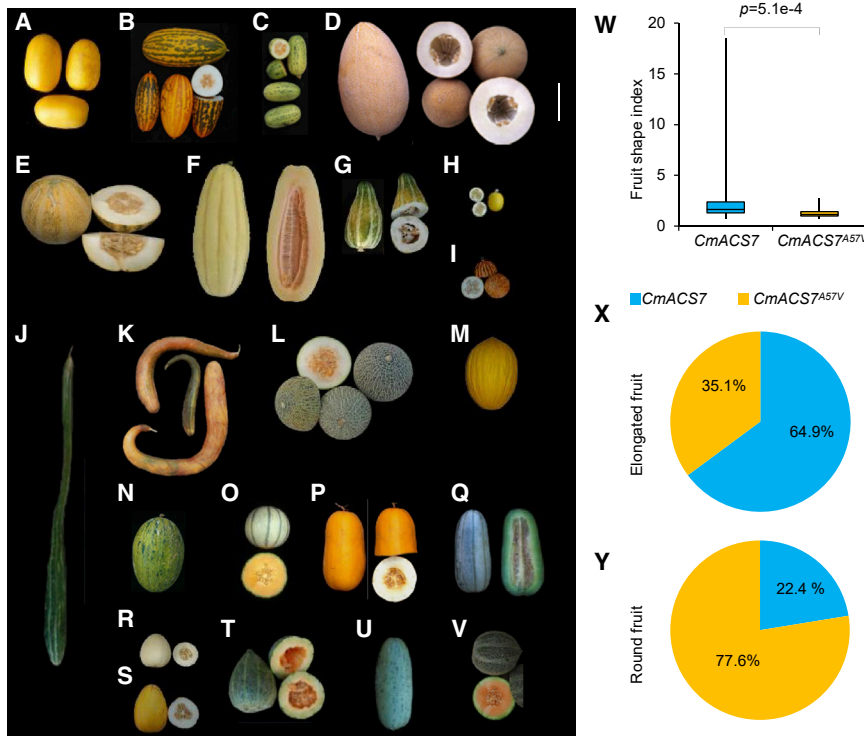


**Figure 2. Round fruit phenotype is associated with *CmACS7*<sup>A57V</sup> allele**

(A–V) Morphological variation of melon fruits from the diversity panel (n = 190) representing 15 horticultural groups. (A and B) *acidulus*, (C) *agrestis*, (D) *ameri*, (E) *chandalak*, (F) *chate*, (G) *chinensis*, (H) *chito*, (I) *dudaim*, (J and K) *flexuosus*, (L–N) *inodorus*, (O) *cantalupensis*, (P) *conomon*, (Q–T) *makuwa*, (U) *momordica*, and (V) *reticulatus*. The picture shows a compilation of fruits from the diversity panel with different colors, shapes, and sizes to illustrate the phenotypic variation present of the fruit shape in melon. For more details, please see [Table S2](#). Scale bars, 10 cm.

(W) Boxplots of fruit shape index. Data are displayed as boxplot whiskers representing  $\pm 1.5 \times$  the interquartile range; horizontal lines, medians.  $p = 5.1 \times 10^{-4}$  (two-tailed Student's t test).

(X and Y) Allele frequencies of *CmACS7* and *CmACS7*<sup>A57V</sup> in melon accessions developing elongated fruits (n = 74) (X) and round fruits (n = 116) (Y).

See also [Table S2](#).

shape. As expected, treated plants developed hermaphrodite flowers and round fruits ([Figure S1T](#)). In summary, these data strongly validate the role of the ethylene produced in the flower by the monoecy genes in the development of elongated fruits.

### ***CmACS7* loss-of-function allele is associated with round fruit melon accessions**

Previously, we have shown that *CmACS7* has a strong selective sweep signal and has experienced a recent positive selection in andromonoecious accessions.<sup>40</sup> To explore the association between *CmACS7*<sup>A57V</sup> loss-of-function allele<sup>40</sup> and fruit shape, we characterized fruit shape in a panel of 190 *Cucumis melo* melon accessions encompassing 15 horticultural groups and 2 sexual types, monoecious and andromonoecious ([Figures 2A–2V](#); [Table S2](#)). At least three fruits per accession were measured, and the average FSi was calculated. Classification according to *CmACS7* or *CmACS7*<sup>A57V</sup> genotype showed that accessions carrying functional *CmACS7* allele develop fruits significantly longer than accessions carrying *CmACS7*<sup>A57V</sup> loss-of-function allele ([Figure 2W](#)). This result was consistent with the comparison of female and hermaphrodite flowers in melon and cucumber ([Figures S1](#) and [S3](#)) and confirmed the role of functional *CmACS7* in elongated fruit development.

We next examined the association of *CmACS7* and *CmACS7*<sup>A57V</sup> alleles relative to FSi ([Figures 2X](#) and [2Y](#)). As observed for the entire panel ([Figure 2W](#)), *CmACS7*<sup>A57V</sup> was strongly enriched in accessions developing round fruit (FSi < 1.5), particularly in the *cantalupensis*, *makuwa*, and *reticulatus* horticultural groups ([Figure 2Y](#); [Table S2](#)). In contrast, most of the elongated fruit accessions carry the WT *CmACS7* allele, and *CmACS7*<sup>A57V</sup> allele is almost absent in the *flexuosus* horticultural group ([Figure 2X](#); [Table S2](#)). In view of the phenotypic association between

cultivated melon accessions is the consequence of the selection of the andromonoecious phenotype.

### **Elongated versus round fruit shapes are determined at stage 8 after flower sex determination**

Characterization of *CmACS7*/*CsACS2* sex transition mutants for fruit shape strongly indicates *Monoecy* gene is pleiotropic, controlling stamen inhibition in female flowers and the development of elongated fruit. To assess whether fruit shape is determined before, during, or after sex determination, we measured OSi of female and hermaphrodite flower buds at different developing stages ([Figure 3](#)). In melon, like in cucumber, female and hermaphrodite flowers at stage 4 are bisexual, developing both stamens and carpel primordia. At stage 6, stamen primordia stop developing in female flowers, leading, at stage 7, to sexually dimorphic female and hermaphrodite flowers.<sup>42</sup> We found no difference in OSi between female and hermaphrodite flower buds until stage 7 ([Figures 3A–3E](#) and [3H](#)). At stage 8, we found ovary length significantly longer in WT compared with *rf1* mutant and no significant difference in the width of the ovaries ([Figures 3F–3I](#)). Based on this, we concluded that elongated versus round fruit shape is determined during ovary development after sex determination. Consistent with this, *CmACS7* is expressed in carpel primordia of flower buds at stage 4, when female and hermaphrodite buds are not morphologically distinguishable.<sup>40</sup> qRT-PCR and *in situ* hybridization show that *CmACS7* is expressed at stage 8, and the accumulation of *CmACS7* mRNA is localized in the central cells of the ovary ([Figures 4B](#) and [4C](#)). Further, *CmACS7* expression level and pattern were not different between female and hermaphrodite flowers ([Figure 4C](#)), a finding consistent with the fact that *rf1* fruit shape is attributed to the loss of *CmACS7* activity ([Figure 1](#)).

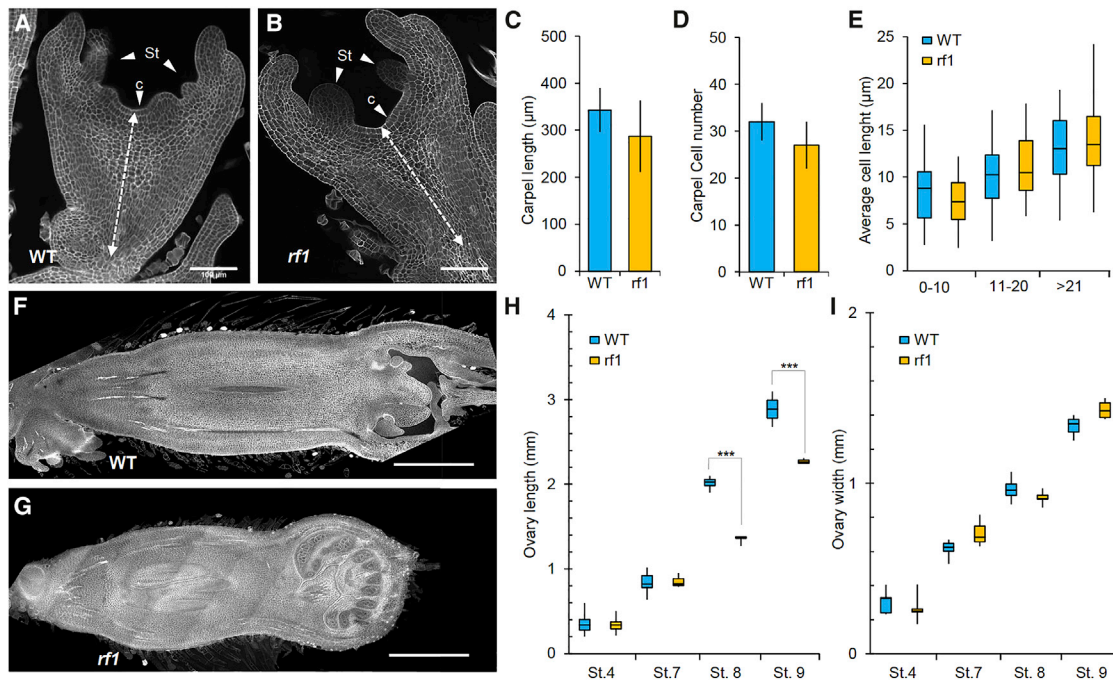


**Figure 3. Fruit shape is determined after sex determination**

(A and B) Confocal images of WT (A) and *rf1* (B) flowers at stage 5 before sexual dimorphism. St, stamen; C, carpel. Scale bars, 100 μm.

(C–E) Carpel length (C), carpel cell number (D), and average cell length (E) in the longitudinal axis of WT and *rf1* flowers at stage 5. Values are mean ± SD derived from 3 flowers.

(F and G) Confocal images of WT (F) and *rf1* (G) flowers at stage 8 after sexual determination. Scale bars, 500 μm.

(H and I) Ovary length (H) and width (I) of WT and *rf1* flowers at different developmental stages (n = 9). Data are displayed as boxplot whiskers representing ±1.5 × the interquartile range; horizontal lines, medians. \*\*\*p < 0.001 (two-tailed Student's t test).

### Developmental and cellular changes leading to fruit shape determination

Organ growth and shape are driven by both cell division and cell growth. These two processes are coordinated but can be independently regulated. To quantify the contribution of the cellular mechanism by which *CmACS7* controls fruit shape, we measured cell numbers and cell sizes along longitudinal and transversal axis of WT female and *rf1* hermaphrodite flowers at stage 8 and at anthesis (Figures 4A, 4L, and 4M). Although female and hermaphrodite flowers differed significantly in ovary length, they do not differ with regard to cell number in the longitudinal axis (Figure 4A). However, cell length was significantly longer in the WT female flowers. In the transversal axis, we observed significantly more cells with smaller length and width in the *rf1* hermaphrodite flowers. These results suggest that *CmACS7* may regulate fruit length by mediating cell expansion and repressing cell division (Figure 4A).

To investigate whether the cell expansion differs uniformly throughout the ovary length, individual cell files along the longitudinal axis of female and hermaphrodite flowers were divided into consecutive sectors of 10 cells and measured (Figure 4E). We observed that the average cell length was similar in the top (cells 1–30) and bottom ovary ends (cells 110 onward) (Figures 4D, 4F, 4G, 4J, and 4K), whereas cells in the sector encompassing the 31<sup>st</sup> to 110<sup>th</sup> cells, expressing *CmACS7*, were significantly longer in female compared with hermaphrodite flowers (Figures 4D, 4H, and 4I).

Endoreduplication is known to be associated with the increase in organ/cell size including fruits.<sup>43–46</sup> To test if the cell size increase in WT compared with *rf1* is due to endoreduplication, we measured the ploidy level of ovary cells of female and hermaphrodite flowers at stage 8 and at anthesis. We observed for both WT and *rf1* flowers similar ploidy levels, indicating that endoreduplication may not contribute to the observed shape difference (Figures 4N and 4O).

Overall, the results demonstrate that *CmACS7*-mediated ethylene biosynthesis positively regulates cell elongation, leading to ovary and thus fruit elongation.

### Ethylene modulates the expression of cell division and cell-elongation-promoting genes

At early fruit developmental stages, *CmACS7* mRNA accumulates in the central cells of the ovary (Figure 4B). To obtain an in-depth resolution of the molecular mechanisms controlling ovary shapes, we examined the transcriptome of laser capture microdissected sequencing (LCM-seq) ovary cells from the central part of female and hermaphrodite flower buds at stages 4 and 8 (Figures 5A–5C). Pairwise comparisons showed that female flowers at stage 8 (G8) are the main contributor of differentially expressed genes (Figures 5D, S4A, and S4B). Overall, we found 2,803 upregulated and 2,363 downregulated genes in G8 (Data S1).

Consistent with the loss of *CmACS7* function explaining the phenotypic variation, we observed many genes involved in the ethylene pathway upregulated in G8 (Figure S4E). We grouped

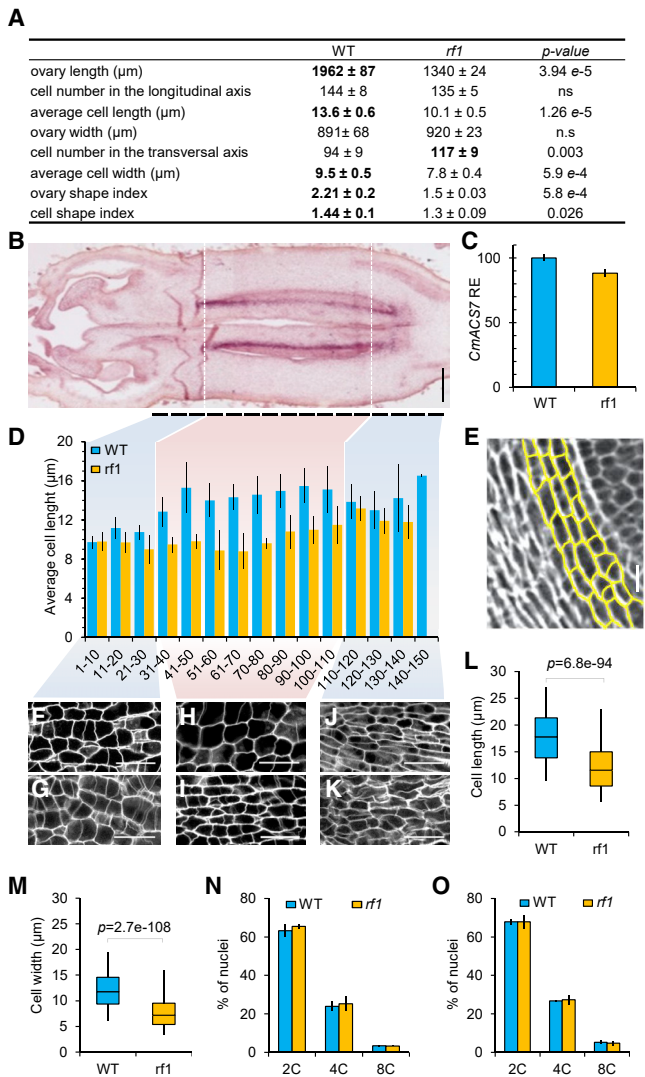


**Figure 4. Cell number and cell length of ovaries from WT and *rf1* flowers**

(A) Characteristics of ovaries from WT and *rf1* flowers. Values are mean ± SD derived from 7 flowers.  
 (B) *CmACS7* *in situ* expression at flower developmental stage 8. Scale bars, 250 μm.  
 (C) Quantitative real-time PCR of *CmACS7* in WT and *rf1* flowers at stage 8. Values are mean ± SD of 3 biological replicates.  
 (D) Cell length averaged from consecutive sectors of 10 cells along the longitudinal axis of the ovary. Values are mean ± SD derived from 5 flowers.  
 (E) Longitudinal cell layers of WT melon flower at stage 8. Scale bars, 10 μm.  
 (F–K) Magnification of the WT (F, H, and J) and *rf1* (G, I, and K) flower cross-section in the apical (F and G), median (H and I), and basal (J and K) ovary regions. Scale bars, 25 μm.  
 (L and M) Boxplots of cell length (L) and cell width (M) at flower anthesis (n = 10). Data are displayed as boxplot whiskers representing ±1.5× the interquartile range; horizontal lines, medians.  
 (N and O) Ploidy analysis by flow cytometry in WT and *rf1* flowers at stage 8 (N) and at anthesis (O). Values are mean ± SD of five biological replicates. Statistical *p* values are calculated using two-tailed Student's *t* test. n.s., not statistically significant difference.  
 See also [Table S3](#).

the differentially expressed genes by their expression patterns into two clusters, reflecting up- or downregulated genes in the G8 samples (Figures 5E, S4C, and S4D). Gene ontology (GO) term enrichment analysis revealed cluster 1 enriched in GO terms related to response to stimulus, chemical, or hormone and cell communication (Figure 5F). In contrast, cluster 2 was enriched in GO terms related to cell division and expansion including translation, DNA metabolic process, cell cycle, cellular process, and microtubule-based movement (Figure 5G). Given the role of cell division and expansion in melon fruit shape, we examined the differentially expressed genes and observed that more than two-thirds of the genes related to cell division (GO:0051301) were downregulated in G8 compared with G4, H4, and H8 samples (Figure S5A), corroborating the reduced number of cells across the ovary width in G8 compared with H8 buds (Figure 4). In contrast, many members of the xyloglucosylate endotransglucosylase/hydrolase (XTH) family, known to govern cell enlargement, were upregulated in G8 compared with H8 buds (Figure S5B). qRT-PCR analysis confirmed the up-regulation of *XTH* genes in G8 (Figures 5H–5K).

Functional annotation further identified several TFs of the *E2F-DP* family downregulated in G8 compared with H8 (Figures S5D and S5E). *E2F-DPs* are TFs known to control cell-cycle transition in both plants and animals.<sup>47–49</sup> In *Arabidopsis*, overexpression of *E2F* has been shown to suppress cell elongation and promotes cell division in cotyledons and hypocotyls.<sup>47,50</sup> Besides, *SWI/SNF-BAF60* TFs, known to inhibit cell elongation in *Arabidopsis* hypocotyl,<sup>51</sup> were also found downregulated in G8 compared with H8 (Figure S5E).

OFPs have been shown to regulate plant organ size. In tomato, rice, and peach, overexpression of *OFP* genes leads to small, rounder fruits.<sup>8,10,19</sup> To regulate cell division and expansion patterns, OFPs interact with Tonneau1 recruitment motif (TRM) proteins.<sup>14</sup> To assess the role of *OFPs* and *TRMs* in melon fruit shape, we have identified 21 *OFP* and 39 *TRM* melon proteins orthologous to *Arabidopsis* and tomato *OFP* and *TRM* proteins (Figures S6A and S6B). Current transcriptomic analysis and qRT-PCR revealed that among the differentially expressed genes, *OFP* gene expression was mainly downregulated in G8 compared with H8 samples (Figures 5L–5O). In contrast, *TRMs* were mainly upregulated in G8 compared with H8 (Figures 5P–5R).

## DISCUSSION

The plant hormone ethylene plays a key role in development, senescence, and adaptation to biotic and abiotic stresses.<sup>52,53</sup> In cucurbits, flower and fruit development can be divided into five major phases: the initiation of floral organs, the sexual dimorphism, the flower anthesis, the fruit development, and the fruit maturation. Ethylene intervenes as a positive and negative regulator through all these developmental phases.<sup>54</sup> Specifically for the flower development phase, we previously showed that ethylene is the key hormonal switch controlling sexual organ development.<sup>40,41,55,56</sup> Here, we demonstrate that ethylene controls fruit shape after the sex determination and before the flower anthesis phase.

Organ shapes (e.g., fruit shape) are the result of coordinated spatiotemporal cell division and expansion. We show that *CmACS7/CsACS2*-mediated ethylene production is necessary

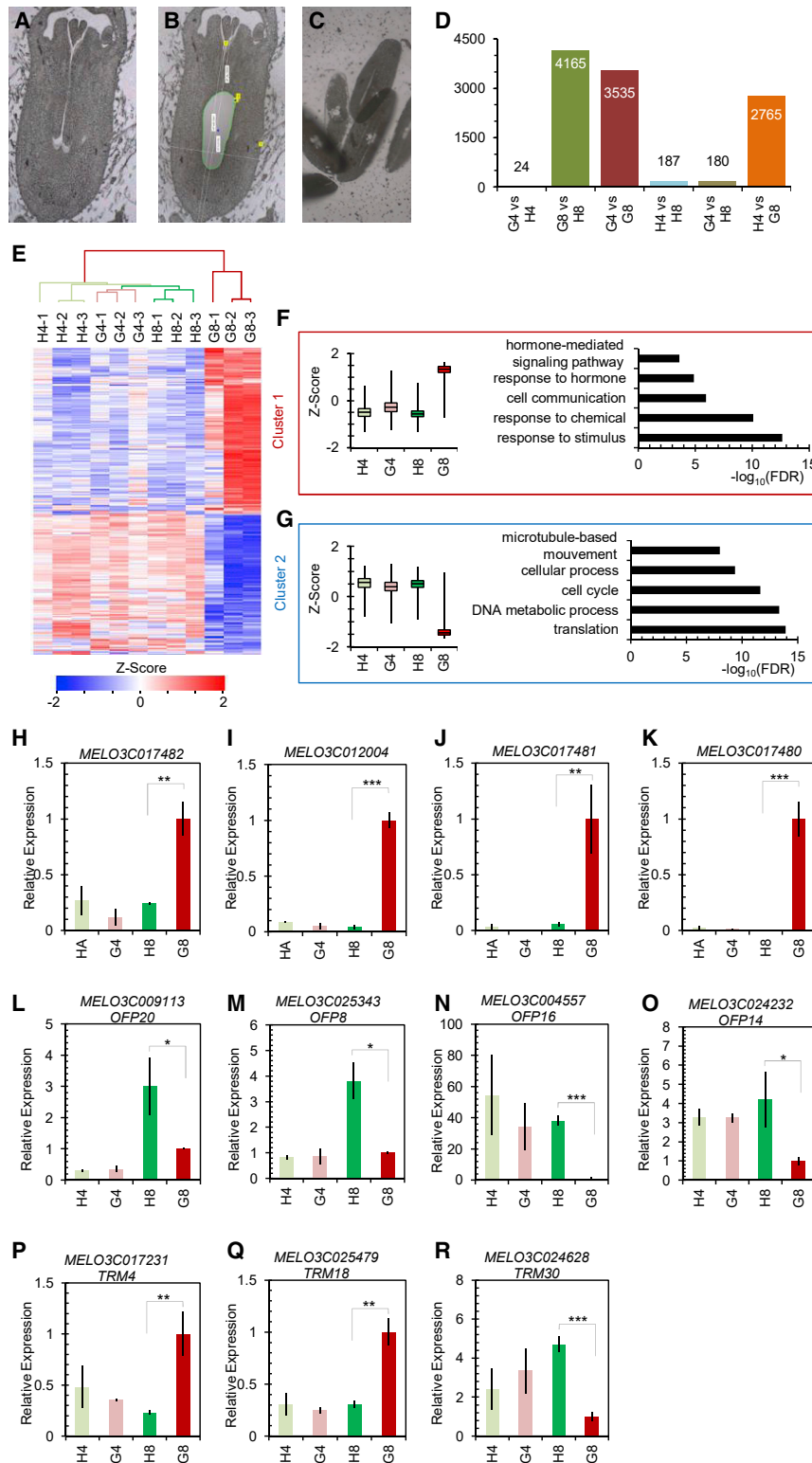


**Figure 5. Gene expression profiling of female and hermaphrodite flowers by LCM-seq**

(A–C) Laser capture microdissection of the ovary median region expressing *CmACS7*.

(D) Differentially expressed genes in pairwise comparison groups.

(E) Gene-wise hierarchical clustering heatmap of all 5,166 differentially expressed genes (adjusted p value < 0.001) showing segregation into two clusters. The Z score scale represents mean-subtracted regularized log-transformed read counts.

(F) Cluster 1 (n = 2,803) includes genes with increased expression in female flowers at stage 8 (G8).

(G) Cluster 2 (n = 2,363) includes genes down-regulated in G8.

Data in (F) and (G) are displayed as boxplot whiskers representing  $\pm 1.5 \times$  the interquartile range; horizontal lines, medians. Enriched GO terms are shown to the right.

(H–R) Quantitative real-time PCR of cell expansion (H–K) and *OFF* (L–O) and *TRM* (P–R) genes in female and hermaphrodite flowers. Values are mean  $\pm$  SD of three biological replicates. \*p < 0.05; \*\*p < 0.01; \*\*\*p < 0.001 (two-tailed Student's t test). H4, hermaphrodite flower at stage 4; G4, female flower at stage 4; H8, hermaphrodite flower at stage 8; G8, female flower at stage 8.

See also [Figures S4–S6](#), [Table S3](#), and [Data S1](#).

for both the development of elongated fruits and female flower development ([Figures 1](#), [S1](#), and [S3](#)), consistent with the mapping of the fruit shape QTL *FS2.2* in the vicinity of the *Monoecy* locus controlling sex determination in melon.<sup>2</sup>

demonstrate that *CmACS7*-mediated fruit shape and sexual determination have been co-selected during melon domestication and further spread by continuous selection of new varieties worldwide. It is important to highlight that even

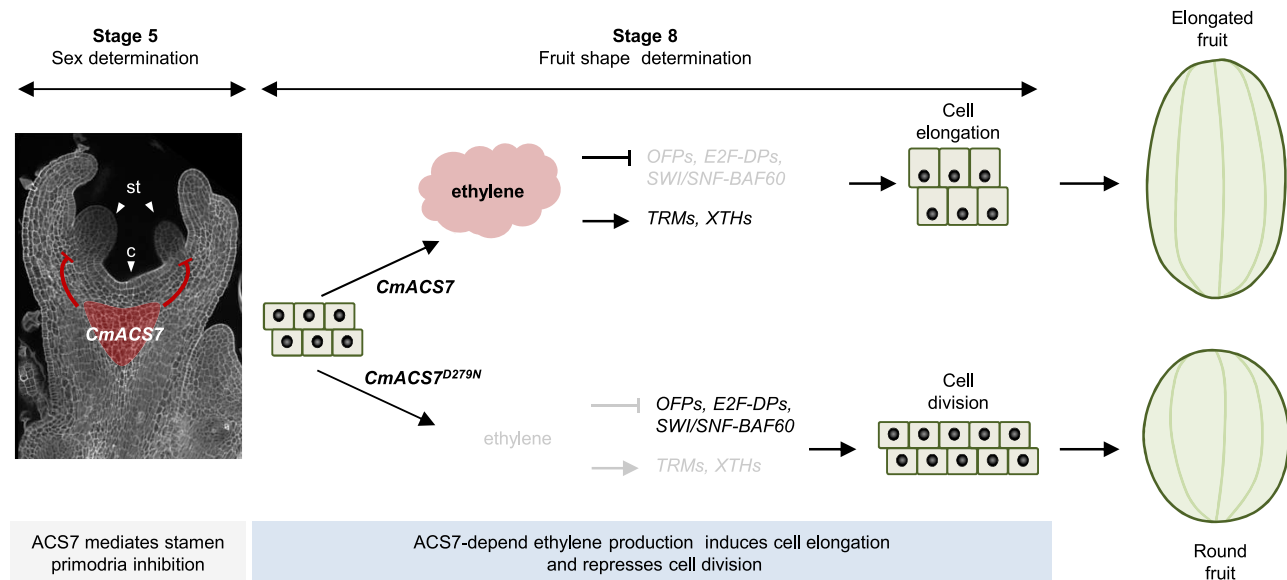


**Figure 6. Proposed model for *CmACS7*-dependent regulation of melon fruit shape**

At developmental stage 5, female and hermaphrodite carpel-bearing flowers express functional or non-functional *CmACS7* protein isoform in the carpel, respectively. Functional *CmACS7* isoform produces ethylene, repressing the development of stamens and leading to the development of female flowers. After sexual differentiation, at stage 8, *CmACS7* continues to be expressed and to produce ethylene in the developing carpels. Ethylene downregulates the expression of *OFP*, *E2F-DP*, and *SWI/SNF-BAF60* genes and induces the expression of *TRM* and *XTH* genes leading to cell elongation and the development of elongated fruit. Expression of the non-functional *CmACS7*<sup>D279N</sup> isoform results in the expression of *OFP*, *E2F-DP*, and *SWI/SNF-BAF60* genes and downregulation of *TRM* and *XTH* genes leading to induced cell division, reduced cell elongation, and finally to the development of round fruit.

though most melon accessions harboring the *CmACS7*<sup>A57V</sup> allele develop round fruits, we found some accessions with the *CmACS7*<sup>A57V</sup> allele developing elongated fruits (Figure 2X). To correct the round shape, melon breeders have screened melon germplasms and identified QTLs that modify fruit shape.<sup>1,27,62</sup> Recently, the melon fruit shape QTL *fsqs8.1/CmFSI8* was shown to encode the *OFP* *CmOFP13*, orthologous to *AtOFP1* and *SIOFP20*.<sup>31,32</sup> Variations at the *CmOFP13* locus could explain the round fruit phenotype observed in melon accessions harboring the *CmACS7* allele (Figure 2Y).

*CmACS7*/*CsACS2* expression inhibits stamen development in a non-cell-autonomous way.<sup>40,41</sup> In contrast, *in situ* expression analysis showed that *CmACS7* expression coincides with the cell enlargement zone in the central region of developing ovaries, pointing toward cell-autonomous control of fruit shape (Figure 4). LCM-seq analysis identified two clusters of gene expression patterns, corresponding to genes upregulated or downregulated in G8, respectively. Consistent with the histological analysis pointing toward inhibition of cell division and enhanced cell elongation as the cause of elongated fruit shape, we found downregulation of *E2F-DPs* and *SWI/SNF-BAF60* TFs known to suppress cell elongation and promote cell division.<sup>47,50,51</sup>

Regulation of microtubule orientation is an important step in cellular regulation of organ shape.<sup>63–66</sup> We found *OFP* genes downregulated and *TRM* genes upregulated in female compared with hermaphrodite flower buds (Figure 5). *TRM* proteins interact with TONNEAU1 (TON1) and protein phosphatase2A (PP2A) to target the TTP (TON1-*TRM*-PP2A) complex to cortical microtubules to delineate the location of the cell division plane.<sup>67–69</sup>

The contrasting expression of *OFP* and *TRM* genes corroborates with the cell size and number differences observed in the fruit shape controlling zone of the ovary. Consistent with this, overexpression of *OFPs* or loss-of-function mutations in *TRMs* resulted in rounder fruits,<sup>8,14,19,67</sup> and QTLs controlling fruit shape were found mapping at the vicinity of *OFP* or *TRM* genes.<sup>14,70,71</sup> In Arabidopsis, overexpression of *AtTRM1* and *AtTRM2* resulted in elongated organs.<sup>72</sup> GO enrichment analysis also revealed major changes in genes related to microtubule-based movement (Figure 5G). The process of cell division and expansion requires dynamic spatial reorganization of microtubule network. Kinesins are a superfamily of microtubule-dependent motor proteins, and they play critical roles in various processes such as cell division and alteration of cell morphology.<sup>73</sup> Surprisingly, transcripts for the majority of the differentially expressed kinesin proteins were found to be downregulated in G8 compared with H8 (Figure S5C). It would be interesting to study the role of kinesins in governing the fruit length, if any. *XTH* enzymes are a large family of cell-wall-modifying enzymes that play a central role in the cell wall expansion and re-modeling. We found a large number of *XTH* enzymes to be upregulated in cells undergoing enlargement. These protein families were also found to be induced by ethylene in rose, arrowhead tubers, and persimmon,<sup>74–76</sup> pointing toward a general mechanism controlling expression of *XTH* enzymes by ethylene.

Treatment of melon plant with an ethylene perception inhibitor, silver nitrate, led to transition from elongated to round ovary and fruit development. In *Ranunculus sceleratus*, ethylene treatment has been shown to promote petiole elongation growth.<sup>77</sup> These two experiments highlight the dual role of ethylene as an inhibitory hormone for cell division rate and a promoting hormone

for cell enlargement. Recently, fine-tuning of ethylene homeostasis through a RING-type E3 ligase was also reported to control cucumber fruit elongation, suggesting conserved mechanisms controlling organ shape in plants.<sup>28</sup>

In summary, we propose a model in which *CmACS7* orchestrates sex determination as well as flower and fruit shape. Expression of *CmACS7* inhibits stamen development in a non-cell-autonomous manner and promotes cell elongation in the carpel to lead to elongated fruit, in a cell-autonomous manner. This process includes activation of cell elongation and inhibition of cell division mechanisms. At the molecular level, ethylene produced locally by *CmACS7* led to repression of cell-division-promoting genes and upregulation of cell-elongation-promoting genes. These processes occur after the flowers acquire their sexual identity and before flower anthesis (Figure 6).

## STAR★METHODS

Detailed methods are provided in the online version of this paper and include the following:

- KEY RESOURCES TABLE
- RESOURCE AVAILABILITY
  - Lead contact
  - Materials availability
  - Data and code availability
- EXPERIMENTAL MODEL AND SUBJECT DETAILS
  - Plant Material
- METHOD DETAILS
  - Measurement of cell number and cell size
  - BSA-Seq Mapping Approach
  - Expression, purification and enzymatic activity assays of recombinant protein
  - Protein structure modeling
  - *In situ* hybridization
  - Identification of OFP and TRM proteins in melon
  - Sequence and phylogeny analysis
  - Silver nitrate treatment
  - Flow Cytometry and ploidy analysis
  - Transcriptome sequencing from laser capture microdissected tissue
  - Hierarchical clustering and GO analysis
  - Reverse transcription polymerase chain reaction (RT-PCR) and qPCR
  - Genotyping
- QUANTIFICATION AND STATISTICAL ANALYSIS

## SUPPLEMENTAL INFORMATION

Supplemental information can be found online at <https://doi.org/10.1016/j.cub.2022.04.031>.

## ACKNOWLEDGMENTS

The authors thank Pascal Audigier, Florie Vion, and Holger Ornstrup for taking care of the plants and the research facilities provided by the Institute of Plant-Science Paris-Saclay (IPS2, France). We thank the Center of Biological Resources CRBLeg of GAFL Avignon for maintaining, characterizing, and providing melon genetic resources and the experimental unit, UE AHM of Avignon, for their technical expertise. We thank Mickael Bourge (flow cytometry platform I2BC) and Cecile Raynaud (IPS2) for their help with the flow cytometry

analysis. Financial support was provided by the European Research Council (ERC-SEXPARTH, 341076), the ANR EPISEX Project (ANR-17-CE20-0019), LabEx Saclay Plant Sciences (SPS) (ANR-10-LABX-40-SPS), and the Plant Biology and Breeding Department of INRAE.

## AUTHOR CONTRIBUTIONS

C.T. and S.F. contributed to the generation of the mutant lines; C.C. contributed to the laser capture microdissection; A. Boualem, S.B., and R.S.D. performed bioinformatic analyses and contributed to the gene expression analysis; S.B. and H.M. performed the cell biology and histological experiments; N.G., C.D., S.F., and A. Boualem carried out the plant phenotyping of melon lines and accessions; and A. Boualem, C.D., and A. Bendahmane conceived and designed the study, supervised the work, analyzed the data, and wrote the manuscript.

## DECLARATION OF INTERESTS

The authors declare no competing interests.

Received: January 5, 2022

Revised: March 21, 2022

Accepted: April 8, 2022

Published: May 6, 2022

## REFERENCES

1. Díaz, A., Zarouri, B., Fergany, M., Eduardo, I., Alvarez, J.M., Picó, B., and Monforte, A.J. (2014). Mapping and introgression of QTL involved in fruit shape transgressive segregation into 'piel de sapo' melon (*Cucumis melo* L.) [corrected]. *PLoS One* 9, e104188.
2. Périn, C., Hagen, L.S., Giovinazzo, N., Besombes, D., Dogimont, C., and Pitrat, M. (2002). Genetic control of fruit shape acts prior to anthesis in melon (*Cucumis melo* L.). *Mol. Genet. Genomics* 266, 933–941.
3. Serquen, F.C., Bacher, J., and Staub, J.E. (1997). Mapping and QTL analysis of horticultural traits in a narrow cross in cucumber (*Cucumis sativus* L.) using random-amplified polymorphic DNA markers. *Mol. Breed.* 3, 257–268.
4. Marguerit, E., Boury, C., Manicki, A., Donnart, M., Butterlin, G., Némorin, A., Wiedemann-Merdinoglu, S., Merdinoglu, D., Ollat, N., and Decroocq, S. (2009). Genetic dissection of sex determinism, inflorescence morphology and downy mildew resistance in grapevine. *Theor. Appl. Genet.* 118, 1261–1278.
5. Doganlar, S., Frary, A., Daunay, M.C., Lester, R.N., and Tanksley, S.D. (2002). Conservation of gene function in the Solanaceae as revealed by comparative mapping of domestication traits in eggplant. *Genetics* 161, 1713–1726.
6. Zygier, S., Chaim, A.B., Efrati, A., Kaluzky, G., Borovsky, Y., and Paran, I. (2005). QTLs mapping for fruit size and shape in chromosomes 2 and 4 in pepper and a comparison of the pepper QTL map with that of tomato. *Theor. Appl. Genet.* 111, 437–445.
7. Zhou, M.X., and Liu, T. (2020). Functional analysis of ovate family proteins (OFPs) in fruit shape formation in strawberry (*Fragaria ananassa*). *Hortscience* 55, S81.
8. Zhou, H., Ma, R.J., Gao, L., Zhang, J.N., Zhang, A.D., Zhang, X.J., Ren, F., Zhang, W.H., Liao, L., Yang, Q.R., et al. (2021). A 1.7-Mb chromosomal inversion downstream of aPpOFP1 gene is responsible for flat fruit shape in peach. *Plant Biotechnol. J.* 19, 192–205.
9. Xu, C., Liberatore, K.L., MacAlister, C.A., Huang, Z., Chu, Y.H., Jiang, K., Brooks, C., Ogawa-Ohnishi, M., Xiong, G., Pauly, M., et al. (2015). A cascade of arabinosyltransferases controls shoot meristem size in tomato. *Nat. Genet.* 47, 784–792.
10. Liu, J.P., Van Eck, J., Cong, B., and Tanksley, S.D. (2002). A new class of regulatory genes underlying the cause of pear-shaped tomato fruit. *Proc. Natl. Acad. Sci. USA* 99, 13302–13306.

11. Muñoz, S., Ranc, N., Botton, E., Bérard, A., Rolland, S., Duffé, P., Carretero, Y., Le Paslier, M.-C., Delalande, C., Bouzayen, M., et al. (2011). Increase in tomato locule number is controlled by two single-nucleotide polymorphisms located near WUSCHEL. *Plant Physiol.* *156*, 2244–2254.
12. Xiao, H., Jiang, N., Schaffner, E., Stockinger, E.J., and van der Knaap, E. (2008). A retrotransposon-mediated gene duplication underlies morphological variation of tomato fruit. *Science* *319*, 1527–1530.
13. Snouffer, A., Kraus, C., and van der Knaap, E. (2020). The shape of things to come: ovate family proteins regulate plant organ shape. *Curr. Opin. Plant Biol.* *53*, 98–105.
14. Wu, S., Zhang, B.Y., Keyhaninejad, N., Rodríguez, G.R., Kim, H.J., Chakrabarti, M., Illa-Berenguer, E., Taitano, N.K., Gonzalo, M.J., Díaz, A., et al. (2018). A common genetic mechanism underlies morphological diversity in fruits and other plant organs. *Nat. Commun.* *9*, 4734.
15. van der Knaap, E., Chakrabarti, M., Chu, Y.H., Clevenger, J.P., Illa-Berenguer, E., Huang, Z.J., Keyhaninejad, N., Mu, Q., Sun, L., Wang, Y.P., and Wu, S. (2014). What lies beyond the eye: the molecular mechanisms regulating tomato fruit weight and shape. *Front. Plant Sci.* *5*, 227.
16. Wu, S., Xiao, H., Cabrera, A., Meulia, T., and van der Knaap, E. (2011). SUN regulates vegetative and reproductive organ shape by changing cell division patterns. *Plant Physiol.* *157*, 1175–1186.
17. Wu, S., Clevenger, J.P., Sun, L., Visa, S., Kamiya, Y., Jikumaru, Y., Blakeslee, J., and van der Knaap, E. (2015). The control of tomato fruit elongation orchestrated by sun, ovate and fs8.1 in a wild relative of tomato. *Plant Sci.* *238*, 95–104.
18. Liu, D., Sun, W., Yuan, Y.W., Zhang, N., Hayward, A., Liu, Y.L., and Wang, Y. (2014). Phylogenetic analyses provide the first insights into the evolution of OVATE family proteins in land plants. *Ann. Bot.* *113*, 1219–1233.
19. Wang, S., Chang, Y., Guo, J., and Chen, J.G. (2007). Arabidopsis ovate family protein 1 is a transcriptional repressor that suppresses cell elongation. *Plant J.* *50*, 858–872.
20. Stepansky, A., Kovalski, I., and Peri-Treves, R. (1999). Intraspecific classification of melons (*Cucumis melo* L.) in view of their phenotypic and molecular variation. *Plant Syst. Evol.* *217*, 313–332.
21. Savage, J.A., Haines, D.F., and Holbrook, N.M. (2015). The making of giant pumpkins: how selective breeding changed the phloem of *Cucurbita maxima* from source to sink. *Plant Cell Environ.* *38*, 1543–1554.
22. Ueda, J., Tanaka, K., and Kato, J. (1986). Plant-growth regulators in *Cucumis melo* L. var. flexuosus Naud fruit during rapid growth. *Plant Cell Physiol.* *27*, 809–818.
23. Paris, H.S. (2016). Germplasm enhancement of *Cucurbita pepo* (pumpkin, squash, gourd: Cucurbitaceae): progress and challenges. *Euphytica* *208*, 415–438.
24. Xu, P., Xu, S.Z., Wu, X.H., Tao, Y., Wang, B.G., Wang, S., Qin, D.H., Lu, Z.F., and Li, G.J. (2014). Population genomic analyses from low-coverage RAD-seq data: a case study on the non-model cucurbit bottle gourd. *Plant J.* *77*, 430–442.
25. Harel-Beja, R., Tzuri, G., Portnoy, V., Lotan-Pompan, M., Lev, S., Cohen, S., Dai, N., Yeselson, L., Meir, A., Libhaber, S.E., et al. (2010). A genetic map of melon highly enriched with fruit quality QTLs and EST markers, including sugar and carotenoid metabolism genes. *Theor. Appl. Genet.* *121*, 511–533.
26. Monforte, A.J., Oliver, M., Gonzalo, M.J., Alvarez, J.M., Dolcet-Sanjuan, R., and Arús, P. (2004). Identification of quantitative trait loci involved in fruit quality traits in melon (*Cucumis melo* L.). *Theor. Appl. Genet.* *108*, 750–758.
27. Monforte, A.J., Diaz, A., Caño-Delgado, A., and van der Knaap, E. (2014). The genetic basis of fruit morphology in horticultural crops: lessons from tomato and melon. *J. Exp. Bot.* *65*, 4625–4637.
28. Xin, T., Zhang, Z., Li, S., Zhang, S., Li, Q., Zhang, Z.H., Huang, S., and Yang, X. (2019). Genetic regulation of ethylene dosage for cucumber fruit elongation. *Plant Cell* *31*, 1063–1076.
29. Zhang, Z., Wang, B., Wang, S., Lin, T., Yang, L., Zhao, Z., Zhang, Z., Huang, S., and Yang, X. (2020). Genome-wide target mapping shows histone deacetylase complex 1 regulates cell proliferation in cucumber fruit. *Plant Physiol.* *182*, 167–184.
30. Zhao, J., Jiang, L., Che, G., Pan, Y., Li, Y., Hou, Y., Zhao, W., Zhong, Y., Ding, L., Yan, S., et al. (2019). A functional allele of *CsFUL1* regulates fruit length through repressing *CsSUP* and inhibiting auxin transport in cucumber. *Plant Cell* *31*, 1289–1307.
31. Ma, J., Li, C., Zong, M., Qiu, Y., Liu, Y., Huang, Y., Xie, Y., Zhang, H., and Wang, J. (2022). CmFSI8/CmOFFP13 encoding an OVATE family protein controls fruit shape in melon. *J. Exp. Bot.* *73*, 1370–1384.
32. Martínez-Martínez, C., Gonzalo, M.J., Sipowicz, P., Campos, M., Martínez-Fernández, I., Leida, C., Zouine, M., Alexiou, K.G., Garcia-Mas, J., Gómez, M.D., et al. (2022). A cryptic variation in a member of the ovate family proteins is underlying the melon fruit shape QTL fsqs8.1. *Theor. Appl. Genet.* *135*, 785–801.
33. Liu, S., Xu, L., Jia, Z., Xu, Y., Yang, Q., Fei, Z., Lu, X., Chen, H., and Huang, S. (2008). Genetic association of ETHYLENE-INSENSITIVE3-like sequence with the sex-determining M locus in cucumber (*Cucumis sativus* L.). *Theor. Appl. Genet.* *117*, 927–933.
34. Rosa, J.T. (1928). The inheritance of flower types in *Cucumis* and *Citrullus*. *Hilgardia* *3*, 233–250.
35. Pan, J., Wang, G., Wen, H.F., Du, H., Lian, H.L., He, H.L., Pan, J.S., and Cai, R. (2018). Differential gene expression caused by the F and M loci provides insight into ethylene-mediated female flower differentiation in cucumber. *Front. Plant Sci.* *9*, 1091.
36. Wang, Y.H., and Irving, H.R. (2011). Developing a model of plant hormone interactions. *Plant Signal. Behav.* *6*, 494–500.
37. Gapper, N.E., McQuinn, R.P., and Giovannoni, J.J. (2013). Molecular and genetic regulation of fruit ripening. *Plant Mol. Biol.* *82*, 575–591.
38. Capitani, G., Hohenester, E., Feng, L., Storici, P., Kirsch, J.F., and Jansonius, J.N. (1999). Structure of 1-aminocyclopropane-1-carboxylate synthase, a key enzyme in the biosynthesis of the plant hormone ethylene. *J. Mol. Biol.* *294*, 745–756.
39. Capitani, G., McCarthy, D.L., Gut, H., Grütter, M.G., and Kirsch, J.F. (2002). Apple 1-aminocyclopropane-1-carboxylate synthase in complex with the inhibitor L-aminoethoxyvinylglycine. Evidence for a ketimine intermediate. *J. Biol. Chem.* *277*, 49735–49742.
40. Boualem, A., Fergany, M., Fernandez, R., Troadec, C., Martin, A., Morin, H., Sari, M.A., Collin, F., Flowers, J.M., Pitrat, M., et al. (2008). A conserved mutation in an ethylene biosynthesis enzyme leads to andromonoecy in melons. *Science* *321*, 836–838.
41. Boualem, A., Troadec, C., Kovalski, I., Sari, M.A., Peri-Treves, R., and Bendahmane, A. (2009). A conserved ethylene biosynthesis enzyme leads to andromonoecy in two *Cucumis* species. *PLoS One* *4*, e6144.
42. Bai, S.L., Peng, Y.B., Cui, J.X., Gu, H.T., Xu, L.Y., Li, Y.Q., Xu, Z.H., and Bai, S.N. (2004). Developmental analyses reveal early arrests of the spore-bearing parts of reproductive organs in unisexual flowers of cucumber (*Cucumis sativus* L.). *Planta* *220*, 230–240.
43. Edgar, B.A., and Orr-Weaver, T.L. (2001). Endoreplication cell cycles: more for less. *Cell* *105*, 297–306.
44. De Veylder, L., Beeckman, T., Beemster, G.T.S., de Almeida Engler, J.D., Ormenese, S., Maes, S., Naudts, M., Van der Schueren, E., Jacqmard, A., Engler, G., and Inzé, D. (2002). Control of proliferation, endoreduplication and differentiation by the Arabidopsis E2Fa-DPa transcription factor. *EMBO J.* *21*, 1360–1368.
45. Gutierrez, C., Ramirez-Parra, E., Castellano, M.M., and del Pozo, J.C. (2002). G(1) to S transition: more than a cell cycle engine switch. *Curr. Opin. Plant Biol.* *5*, 480–486.
46. Harbour, J.W., and Dean, D.C. (2000). The Rb/E2F pathway: expanding roles and emerging paradigms. *Genes Dev.* *14*, 2393–2409.

47. Ramirez-Parra, E., López-Matas, M.A., Fründt, C., and Gutierrez, C. (2004). Role of an atypical E2F transcription factor in the control of Arabidopsis cell growth and differentiation. *Plant Cell* 16, 2350–2363.
48. Jégu, T., Veluchamy, A., Ramirez-Prado, J.S., Rizzi-Paillet, C., Perez, M., Lhomme, A., Latrasse, D., Coleno, E., Vicaire, S., Legras, S., et al. (2017). The Arabidopsis SWI/SNF protein BAF60 mediates seedling growth control by modulating DNA accessibility. *Genome Biol.* 18, 114.
49. Cheniclet, C., Rong, W.Y., Causse, M., Frangne, N., Bolling, L., Carde, J.P., and Renaudin, J.P. (2005). Cell expansion and endoreduplication show a large genetic variability in pericarp and contribute strongly to tomato fruit growth. *Plant Physiol.* 139, 1984–1994.
50. Mauxion, J.P., Chevalier, C., and Gonzalez, N. (2021). Complex cellular and molecular events determining fruit size. *Trends Plant Sci.* 26, 1023–1038.
51. Renaudin, J.P., Deluche, C., Cheniclet, C., Chevalier, C., and Frangne, N. (2017). Cell layer-specific patterns of cell division and cell expansion during fruit set and fruit growth in tomato pericarp. *J. Exp. Bot.* 68, 1613–1623.
52. Khan, N.A., Khan, M.I.R., Ferrante, A., and Poor, P. (2017). Editorial: Ethylene: a key regulatory molecule in plants. *Front. Plant Sci.* 8, 1782.
53. Park, C., Lee, H.Y., and Yoon, G.M. (2021). The regulation of ACC synthase protein turnover: a rapid route for modulating plant development and stress responses. *Curr. Opin. Plant Biol.* 63, 102046.
54. Iqbal, N., Khan, N.A., Ferrante, A., Trivellini, A., Francini, A., and Khan, M.I.R. (2017). Ethylene role in plant growth, development and senescence: interaction with other phytohormones. *Front. Plant Sci.* 8, 475.
55. Boualem, A., Troadec, C., Camps, C., Lemhemi, A., Morin, H., Sari, M.A., Fraenkel-Zagouri, R., Kovalski, I., Dogimont, C., Perl-Treves, R., and Bendahmane, A. (2015). A cucurbit androecy gene reveals how unisexual flowers develop and dioecy emerges. *Science* 350, 688–691.
56. Boualem, A., Lemhemi, A., Sari, M.A., Pignoly, S., Troadec, C., Abou Choucha, F., Solmaz, I., Sari, N., Dogimont, C., and Bendahmane, A. (2016). The andromonoecious sex determination gene predates the separation of *Cucumis* and *Citrullus* Genera. *PLoS One* 11, e0155444.
57. Kirkbride, J.H. (1993). *Biosystematic Monograph of the Genus Cucumis (Cucurbitaceae)* (Parkway Publishers).
58. Miller, J.S., and Diggle, P.K. (2003). Diversification of andromonoecy in Solanum section Lasiocarpa (Solanaceae): the roles of phenotypic plasticity and architecture. *Am. J. Bot.* 90, 707–715.
59. Lloyd, D.G. (1980). Sexual strategies in plants. I. An hypothesis of serial adjustment of maternal investment during one reproductive session. *New Phytol.* 86, 69–79.
60. Bertin, R.I. (1982). The evolution and maintenance of andromonoecy. *Evol. Theory* 6, 25–32.
61. Vallejo-Marin, M., and Rausher, M.D. (2007). The role of male flowers in andromonoecious species: energetic costs and siring success in *Solanum carolinense* L. *Evolution* 61, 404–412.
62. Pereira, L., Ruggieri, V., Pérez, S., Alexiou, K.G., Fernández, M., Jahrmann, T., Pujol, M., and Garcia-Mas, J. (2018). QTL mapping of melon fruit quality traits using a high-density GBS-based genetic map. *BMC Plant Biol.* 18, 324.
63. Lazzaro, M.D., Wu, S., Snouffer, A., Wang, Y., and van der Knaap, E. (2018). Plant organ shapes are regulated by protein interactions and associations with microtubules. *Front. Plant Sci.* 9, 1766.
64. Marchant, H.J. (1979). Microtubules, cell wall deposition and the determination of plant-cell shape. *Nature* 278, 167–168.
65. Shibaoka, H. (1994). Plant hormone-induced changes in the orientation of cortical microtubules: alterations in the cross-linking between microtubules and the plasma-membrane. *Annu. Rev. Plant. Physiol. Plant. Mol. Biol.* 45, 527–544.
66. Roberts, I.N., Lloyd, C.W., and Roberts, K. (1985). Ethylene-induced microtubule reorientations: mediation by helical arrays. *Planta* 164, 439–447.
67. Drevensek, S., Goussot, M., Duroc, Y., Christodoulidou, A., Steyaert, S., Schaefer, E., Duvernois, E., Grandjean, O., Vantard, M., Bouchez, D., and Pastuglia, M. (2012). The Arabidopsis TRM1-TON1 interaction reveals a recruitment network common to plant cortical microtubule arrays and eukaryotic centrosomes. *Plant Cell* 24, 178–191.
68. Azimzadeh, J., Nacry, P., Christodoulidou, A., Drevensek, S., Camilleri, C., Amieur, N., Parcy, F., Pastuglia, M., and Bouchez, D. (2008). Arabidopsis TONNEAU1 proteins are essential for preprophase band formation and interact with centrin. *Plant Cell* 20, 2146–2159.
69. Spinner, L., Gadeyne, A., Belcram, K., Goussot, M., Moison, M., Duroc, Y., Eeckhout, D., De Winne, N., Schaefer, E., Van de Slijke, E., et al. (2013). A protein phosphatase 2A complex spatially controls plant cell division. *Nat. Commun.* 4, 1863.
70. Xanthopoulou, A., Montero-Pau, J., Mellidou, I., Kissoudis, C., Blanca, J., Picó, B., Tsballa, A., Tsaliki, E., Dalakouras, A., Paris, H.S., et al. (2019). Whole-genome resequencing of *Cucurbita pepo* morphotypes to discover genomic variants associated with morphology and horticulturally valuable traits. *Hortic. Res.* 6, 94.
71. Colle, M., Weng, Y.Q., Kang, Y.Y., Ophir, R., Sherman, A., and Grumet, R. (2017). Variation in cucumber (*Cucumis sativus* L.) fruit size and shape results from multiple components acting pre-anthesis and post-pollination. *Planta* 246, 641–658.
72. Lee, Y.K., Kim, G.T., Kim, I.J., Park, J., Kwak, S.S., Choi, G., and Chung, W.I. (2006). LONGIFOLIA1 and LONGIFOLIA2, two homologous genes, regulate longitudinal cell elongation in Arabidopsis. *Development* 133, 4305–4314.
73. Nebenführ, A., and Dixit, R. (2018). Kinesins and myosins: molecular motors that coordinate cellular functions in plants. *Annu. Rev. Plant Biol.* 69, 329–361.
74. Ookawara, R., Satoh, S., Yoshioka, T., and Ishizawa, K. (2005). Expression of alpha-expansin and xyloglucan endotransglucosylase/hydrolase genes associated with shoot elongation enhanced by anoxia, ethylene and carbon dioxide in arrowhead (*Sagittaria pygmaea* Miq.) tubers. *Ann. Bot.* 96, 693–702.
75. Singh, A.P., Dubey, S., Lakhwani, D., Pandey, S.P., Khan, K., Dwivedi, U.N., Nath, P., and Sane, A.P. (2013). Differential expression of several xyloglucan endotransglucosylase/hydrolase genes regulates flower opening and petal abscission in roses. *AoB Plants* 5, plt030.
76. Zhu, Q.G., Zhang, Z.K., Rao, J.P., Huber, D.J., Lv, J.Y., Hou, Y.L., and Song, K.H. (2013). Identification of xyloglucan endotransglucosylase/hydrolase genes (XTHs) and their expression in persimmon fruit as influenced by 1-methylcyclopropene and gibberellic acid during storage at ambient temperature. *Food Chem.* 138, 471–477.
77. Smulders, M.J.M., and Horton, R.F. (1991). Ethylene promotes elongation growth and auxin promotes radial growth in *Ranunculus sceleratus* petioles. *Plant Physiol.* 96, 806–811.
78. Dahmani-Mardas, F., Troadec, C., Boualem, A., Lévêque, S., Alsadon, A.A., Aldoss, A.A., Dogimont, C., and Bendahmane, A. (2010). Engineering melon plants with improved fruit shelf life using the TILLING approach. *PLOS ONE* 5, e15776.
79. Boualem, A., Fleurier, S., Troadec, C., Audigier, P., Kumar, A.P.K., Chatterjee, M., Alsadon, A.A., Sadler, M.T., Wahb-Allah, M.A., Al-Doss, A.A., and Bendahmane, A. (2014). Development of a *Cucumis sativus* TILLInG platform for forward and reverse genetics. *PLoS One* 9, e97963.
80. Garcia-Mas, J., Benjak, A., Sanseverino, W., Bourgeois, M., Mir, G., González, V.M., Hénaff, E., Câmara, F., Cozzuto, L., Lowy, E., et al. (2012). The genome of melon (*Cucumis melo* L.). *Proc. Natl. Acad. Sci. USA* 109, 11872–11877.
81. Huai, Q., Xia, Y., Chen, Y., Callahan, B., Li, N., and Ke, H. (2001). Crystal structures of 1-aminocyclopropane-1-carboxylate (ACC) synthase in complex with aminoethoxyvinylglycine and pyridoxal-5'-phosphate provide new insight into catalytic mechanisms. *J. Biol. Chem.* 276, 38210–38216.
82. Pedroza-García, J.A., Domenichini, S., Mazubert, C., Bourge, M., White, C., Hudik, E., Bounon, R., Tariq, Z., Delannoy, E., del Olmo, I., et al.

- (2016). Role of the polymerase  $\epsilon$  sub-unit DPB2 in DNA replication, cell cycle regulation and DNA damage response in *Arabidopsis*. *Nucleic Acids Res.* *44*, 7251–7266.
83. Tyanova, S., and Cox, J. (2018). Perseus: a bioinformatics platform for integrative analysis of proteomics data in cancer research. *Methods Mol. Biol.* *1711*, 133–148.
84. Tian, T., Liu, Y., Yan, H.Y., You, Q., Yi, X., Du, Z., Xu, W.Y., and Su, Z. (2017). agriGO v2.0: a GO analysis toolkit for the agricultural community, 2017 update. *Nucleic Acids Res.* *45*, W122–W129.
85. Eleblu, J.S.Y., Haraghi, A., Mania, B., Camps, C., Rashid, D., Morin, H., Dogimont, C., Boualem, A., and Bendahmane, A. (2019). The gynoeocious CmWIP1 transcription factor interacts with CmbZIP48 to inhibit carpel development. *Sci. Rep.* *9*, 15443.

STAR★METHODS

KEY RESOURCES TABLE

REAGENT or RESOURCE	SOURCE	IDENTIFIER
<b>Bacterial and virus strains</b>		
<i>E. coli</i> BL21(DE3)pLysS	ThermoFisher Scientific	Cat#C6066010
<b>Biological samples</b>		
Melon accessions	This paper	Institute of Plant of Paris –Saclay (IPS2)
<b>Chemicals, peptides, and recombinant proteins</b>		
RNase A	Qiagen	Cat#19101
1X TE Buffer	ThermoFisher Scientific	Cat#12090015
RCL2	Excilone	Cat#01250129
PEN-membrane glass slides	ThermoFisher Scientific	Cat#LCM0522
DNase/RNase-Free Distilled Water	ThermoFisher Scientific	Cat#15667708
RiboLock RNase Inhibitor (40 U/μL)	ThermoFisher Scientific	Cat#EO0381
Phenol/Chloroform/Isoamyl Alcohol, 25:24:1 (v/v)	Sigma-Aldrich	Cat#516726
Sodium Acetate (3 M), pH 5.5, RNase-free	ThermoFisher Scientific	Cat#AM9740
SuperScript IV Reverse Transcriptase	ThermoFisher Scientific	Cat#18090010
Tris-HCl Buffer, pH 8 (1 M)	ThermoFisher Scientific	Cat#BP1758
EDTA (500 mM)	ThermoFisher Scientific	Cat#15575
Alu1	New England Biolabs	Cat#R0137S
rCutSmart Buffer	New England Biolabs	Cat# B6004SVIAL
Taq polymerase	New England Biolabs	Cat#M0267S
10X ThermoPol Rxn Buffer	New England Biolabs	Cat#B9004S
<b>Critical commercial assays</b>		
PicoPure RNA Isolation Kit	Excilone	Cat#KIT0204
SMARTer Ultra Low RNA Kit	Clontech	Cat#634936
TruSeq SBS Kit v3-HS	Illumina	Cat#FC-401-3001
<b>Deposited data</b>		
LCM RNA-seq dataset of female and hermaphrodite <i>C.melo</i> charmono flowers	This paper	SRA: PRJNA814521
<b>Oligonucleotides</b>		
Primers used for this experiment are listed in Table S3.	N/A	N/A
<b>Software and algorithms</b>		
ClustalW	<a href="http://www.ebi.ac.uk/Tools/clustalw2">http://www.ebi.ac.uk/Tools/clustalw2</a>	N/A
MEGAX	<a href="http://www.megasoftware.net/index.html">http://www.megasoftware.net/index.html</a>	N/A
STAR 2.7.3a	<a href="https://github.com/alexdobin/STAR">https://github.com/alexdobin/STAR</a>	N/A
featureCounts	<a href="https://bioinformaticshome.com/tools/rna-seq/descriptions/FeatureCounts.html">https://bioinformaticshome.com/tools/rna-seq/descriptions/FeatureCounts.html</a>	N/A
DESeq2	<a href="https://bioconductor.org/packages/release/bioc/html/DESeq2.html">https://bioconductor.org/packages/release/bioc/html/DESeq2.html</a>	N/A
<b>Other</b>		
Palm DIC FLUO Microdissection System	ZEISS	N/A
Agilent 2100 bioanalyzer	Agilent Technologies	<a href="https://www.agilent.com/en/product/automated-electrophoresis/bioanalyzer-systems/bioanalyzer-instrument/2100-bioanalyzer-instrument-228250">https://www.agilent.com/en/product/automated-electrophoresis/bioanalyzer-systems/bioanalyzer-instrument/2100-bioanalyzer-instrument-228250</a>

(Continued on next page)

**Continued**

REAGENT or RESOURCE	SOURCE	IDENTIFIER
Bionano Genomics Irys System	Bionano Genomics	Cat#IN-011-01
Confocal microscope	ZEISS	Cat#LM880
Diagenode Bioruptor 200 UCD-300	Diagenode	Cat# B01020001

**RESOURCE AVAILABILITY**

**Lead contact**

Further information and requests for resources and reagents should be directed to and will be fulfilled by the Lead Contact, Abdelhafid Bendahmane ([abdelhafid.bendahmane@inrae.fr](mailto:abdelhafid.bendahmane@inrae.fr)).

**Materials availability**

This study did not generate new unique reagents.

**Data and code availability**

Accession numbers are listed in the [key resources table](#). This paper does not report original code. The high-throughput sequencing datasets generated in this study have been deposited in the Sequence Read Archive (SRA) under the accession number SRA: PRJNA814521. Other data supporting our findings are available in the manuscript file or from the corresponding author upon request.

**EXPERIMENTAL MODEL AND SUBJECT DETAILS**

**Plant Material**

The seeds of Charentais Mono line of melon (*Cucumis melo* L.) were treated with ethyl methanesulfonate (EMS) as described in Dahmani-Mardas et al.<sup>78</sup> The M1 plants were self-pollinated, and the round fruit line *rf1* was identified in the M2 population. Then, *rf1* was crossed with the Charentais Mono line and an F2 population was derived from self-crossed F1 plants. Mutant melon lines harboring either of the CmACS7<sup>D376N</sup>, CmACS7<sup>G19E</sup> and CmACS7<sup>A57V</sup> were used in this study.<sup>40</sup> Similarly, cucumber wild-type and mutant lines harboring either of the CsACS2<sup>G33C</sup>, CsACS2<sup>S238F</sup>, CsACS2<sup>S249F</sup>, CsACS2<sup>P209S</sup> and CsACS2<sup>S399L</sup> were also used in this study.<sup>41,79</sup> Plants were grown in the greenhouse in the spring and summer under standard agronomic conditions and evaluated for flower sex type and fruit shape during three consecutive growing seasons. For the 190 melon accessions of the diversity panel, encompassing 15 horticultural groups and monoecious and andromonoecious sexual types, were grown at INRAE GAFL Avignon station. 2 plants for each accession were phenotyped and 3 fruits per plant were scored for mature fruit length, diameter and shape index. Representative fruits from each accession are shown in [Figures 2A–2V](#).

**METHOD DETAILS**

**Measurement of cell number and cell size**

To measure the ovary cell size and number, fresh-picked flower buds from Charentais Mono and *rf1* plants were sampled at different developmental stages 4, 7, 8 and 9 and fixed in FAE solution (formaldehyde: acetic acid: 70% ethanol; 1:1:18 ration) for 24 hours and then washed four times with 70% ethanol. For the measurements, flower buds were stained with 0.1 mM propidium iodide (Sigma-Aldrich) for 1 hour and longitudinal images were recorded using the Zeiss LSM 880 confocal microscope. The cell size and number were then calculated using Image J software. The means and standard errors were calculated from the measurements of at least 5 flower buds for each genotype. Student's t test was used to compare the cell number and cell size difference between the WT and *rf1* plants.

**BSA-Seq Mapping Approach**

To map the *rf1* causal mutation, an F2 population was constructed by crossing *rf1* mutant plant with WT Charentais Mono plant. More than 200 F2 plants were phenotyped and sampled for individual genomic DNA extraction. Mutant and WT pools were created by mixing equal ratio of genomic DNA from round-fruit and elongated-fruit F2 plants. Genomic DNA pools were shared for preparation of sequencing libraries following the recommendation of Illumina TruSeq DNA PCR-free prep kit. Reads of the two bulks (mutant and WT) were aligned to the reference melon genome.<sup>80</sup> For each bulk, the SNP-index across all loci was calculated as the proportion of reads that were different from the reference allele. The delta ( $\Delta$ ) SNP-index was calculated by subtracting the SNP-indices of the two bulks at each locus (SNP-index<sub>mutant</sub> – SNP-index<sub>WT</sub>).

**Expression, purification and enzymatic activity assays of recombinant protein**

Recombinant proteins, CmACS7 and CmACS7<sup>D279N</sup>, were expressed, purified and assayed as described in Boualem et al.<sup>40</sup> Briefly, CmACS7 cDNAs from monoecious, and CmACS7<sup>D279N</sup> TILLING mutant were cloned in pET-15b vector as His6-tagged proteins and

expressed in *E. coli* BL21(DE3)pLysS cells. Protein expression was induced by adding IPTG (0.5 mM) and cells were grown for 5 hours at 25°C. Cells were harvested and disrupted on ice by sonication in the lysis buffer using five pulses of 30 seconds at 20 kHz with 3 minutes cooling on ice between each pulse. The supernatant separated from cell debris was applied to a Ni-IDA 15 ml column (Sigma, France). Wild type (CmACS7) and mutant (CmACS7<sup>D279N</sup>) forms of protein were then eluted with the same buffer. CmACS7 and CmACS7<sup>D279N</sup> enzyme activity was determined by monitoring the MTA formation. Specific activity measurement was performed on 3 different enzyme preparations. Specific activities were measured on dialyzed enzymes in the presence of 60 μM SAM and various PLP concentrations. Residual activities (%) corresponds to the specific activity measured / specific activity measured for CmACS7 enzyme at 300 μM PLP.

### Protein structure modeling

The CmACS7 three-dimensional structures were generated using the Geno3D server (<http://geno3d-pbil.ibcp.fr>). Superposition of the tomato ACS structure (1IAY.pdb) determined by x-ray crystallography<sup>81</sup> and the CmACS7 model was carried out and visualized using the Chimera server (<http://www.cgl.ucsf.edu/chimera>).

### In situ hybridization

CmACS7 in situ hybridization was performed as described in Boualem et al.<sup>40</sup> Primers used for this experiment are listed in [Table S3](#).

### Identification of OFP and TRM proteins in melon

To identify candidate OFP and TRM proteins, the melon database (<http://www.cucurbitgenomics.org/>) was searched first using the keywords 'OFP' or 'TRM'. In addition, Arabidopsis and tomato OFP and TRM protein sequences were downloaded from The Arabidopsis Information Resource (<http://www.arabidopsis.org/>) and the Sol Genomics Network (<http://solgenomics.net/>), respectively. These sequences were used to identify homologous peptides from melon by performing a BLASTP search at melon genome v3.5 database (<http://cucurbitgenomics.org/>). The BLAST E-value was set to 1e−3. Finally, repeated and incomplete sequences were removed manually and the non-redundant CmOFP and CmTRM sequences were subjected to further analyses.

### Sequence and phylogeny analysis

Multiple sequence alignment of full-length protein sequences of CmACS7 with homologous proteins from *Cucumis sativus* (Cs), *Vitis vinifera* (Vv), *Cucurbita maxima* (Cmax), *Arabidopsis thaliana* (At), *Solanum lycopersicum* (Sl), *Petunia hybrida* (Ph), *Medicago truncatula* (Mt), *Momordica charantia* (Mc), *Triticum aestivum* (Ta) and *Picea glauca* (Pg) was performed using the ClustalW (<http://www.ebi.ac.uk/Tools/clustalw2>). Phylogenetic trees were constructed by MEGAX (<http://www.megasoftware.net/index.html>) based on the Neighbor-Joining method.

### Silver nitrate treatment

To assess the effect of AgNO<sub>3</sub> on fruit shape, 400 ppm of the ethylene perception inhibitor, AgNO<sub>3</sub> solution was periodically sprayed on the leaves of WT Charentais Mono line at 20 internodes developmental stage. About 3 weeks after treatment, perfect flowers appeared and were selfed. The fruits developed from AgNO<sub>3</sub>-induced hermaphrodite flowers were phenotyped for fruit shape index.

### Flow Cytometry and ploidy analysis

To determine the flower ploidy level, young flower buds at stage 8 was chopped with a new razor blade in 1 ml of nuclei-isolation buffer.<sup>82</sup> Suspended nuclei were filtered through a 40-μm Fisher brand cell strainer, treated with RNase (5U/mL), and stained with propidium iodide (0.001 μg/100 μL sample). Ploidy level of ~10,000 nuclei was determined using a Cyflow SL3 flow cytometer (Partec-Sysmex). Ploidy histograms were quantitatively analyzed with DPAC software (Partec).

### Transcriptome sequencing from laser capture microdissected tissue

Transcriptomic analysis was carried out on laser capture microdissected central region of carpels for both female and hermaphrodite flowers from the WT Charentais Mono and *rf1* plants, respectively. Two different developmental stages (stages 4 and 8) were chosen such that the transcriptomic profiles can be compared before and after the divergence in ovary shape index (OSi) between the female and hermaphrodite flowers. Female and hermaphrodite flower buds at stage 4 were referred to as G4 and H4, respectively. Female and hermaphrodite flower buds at stage 8 were referred to as G8 and H8, respectively.

### Tissue embedding

Flowers buds were fixed in RCL2 (Excilone) with 0.01% triton. For tissue fixation, samples were placed under vacuum 4 times for 15 min and kept in the fixative overnight at 4 °C. Samples were then dehydrated at 4 °C in a graded series of ethanol (70% for 30 min, 96% for 30 min, 100% for 3 × 30 min), followed by a graded series of ethanol:histoclear bath (3:1, 1:1, 1:3 for 1 h each). Histoclear was then substituted by Surgipath Paraplast Plus tissue embedding media (Leica Biosystems) and incubated overnight at 60 °C. Finally, flowers were embedded into paraffin blocks, cooled and stored at −20 °C.

### Laser capture microdissection

A Rotary microtome (HM 3555 Microtom) was used to cut 8 μm thick longitudinal sections of the embedded flowers. Ribbon of flower sections were stretched on UV-treated, 1 mm PEN-membrane covered slides (Arcturus Bioscience, Excilone) such that each slide

corresponds to 15–25 sections of flowers. Slides were deparaffinized, and laser capture microdissection was immediately conducted on a Palm DIC FLUO Microdissection System (Zeiss). The contours of central carpel sector encompassing the 31<sup>st</sup> to 110<sup>th</sup> cells were cut with the laser and target regions were catapulted into Adhesive cap 500 clear (Zeiss).

#### **RNA extraction**

Immediately after dissection, cells were lysed using the PicoPure RNA Isolation Kit (Arcturus Bioscience, Excilone) and stored at –20 °C before RNA extraction. RNA quality and concentration were evaluated with a Bioanalyser 2100 (Agilent Technologies) on Agilent RNA Pico chips. RNA recovery ranged from 900–2000 pg/μl, with a RIN above 7.

#### **Preparation of the sequencing libraries**

2 ng of total RNA was used for each cDNA library preparation using the SMARTer Ultra Low RNA Kit for Illumina Sequencing from Clontech according to manufacturer's instructions. Libraries were sequenced on the HiSeq2000 platform Illumina and 30 to 50 million paired-end reads per sample were obtained. Read quality was assessed using FastQC (version 0.11) and STAR (version 2.7) has been used to generate the mapping files. The mapped reads were assigned to genes with featureCount (v2.0.0). DESeq2 (version 1.30.1) was used to identify the differentially expressed (DE) genes (adjusted p value <0.001 and log<sub>2</sub>(FC)>1 or <-1).

#### **Hierarchical clustering and GO analysis**

The DE genes were subjected to hierarchical clustering analysis using Perseus to identify the co-expressed DE genes<sup>83</sup> GO enrichment analysis was performed on AgriGOv2 web server.<sup>84</sup>

#### **Reverse transcription polymerase chain reaction (RT-PCR) and qPCR**

For the RT-qPCR, the total RNAs from laser capture microdissection experiments were used to validate the gene expression pattern. Primer design was performed with the Primer3 software ([http://frodo.wi.mit.edu/cgi-bin/primer3/primer3\\_www.cgi](http://frodo.wi.mit.edu/cgi-bin/primer3/primer3_www.cgi)). Primers sequences are listed in [Table S3](#). To check specificity of the designed primers, all amplicons were sequenced and blasted against NCBI database. Polymerase chain reactions were performed in an optical 384-well plate with the Bio-Rad CFX96 Real-time PCR apparatus, with qPCR MasterMix Plus for SYBR Green I w/o ROX (Eurogentec) and according to manufacturer's instructions. PCR amplification specificity was verified by a dissociation curve (55 °C to 95 °C). A negative control without cDNA, technical replicates on three independent synthesis of cDNA (derived from the same RNA sample), and three independent biological experiments were performed in all cases. Gene expression is normalized to the expression levels of housekeeping genes: *CmActin2* and *CmADP* (primers shown in [Table S3](#)). The gene relative expressions were determined as described in Eleblu et al.<sup>85</sup>

#### **Genotyping**

The genotyping of 81 melons accessions for the C to T nucleotide transition leading to A57V amino acid substitution was carried out with the cleaved amplified polymorphic sequence (CAPS) marker described in Boualem et al.<sup>40</sup> and on the basis of *Alu1* restriction site polymorphism. Briefly, melon genomic DNA was extracted from young leaves following CTAB method and was used as matrix for *CmACS7* PCR amplification using primers described in [Table S3](#). PCR products were then digested by *Alu I* restriction enzyme to assess the presence absence of the C to T nucleotide transition.

### **QUANTIFICATION AND STATISTICAL ANALYSIS**

For the fruit and ovary shape phenotypic analysis in WT Charentais Mono and *rf1* plants, 10 fruits from at least 5 independent plants for ch genotype were analyzed. For the ovary shape phenotypic analysis, 20 flowers at anthesis from at least 5 independent plants for each genotype were analyzed.

Statistical significance analysis between two groups was performed using the Student's t test.

For RNA-seq analysis, pool of laser captured microdissected samples from 3 flower buds has been used as one biological replicate. Three biological replicates were performed for RNA-seq. For RT-qPCR analysis, the expression values correspond to the average of three biological replicates, with three technical replicates.